Nuclear Instruments and Methods in Physics Research A239 (1985) 536–544
North-Holland, Amsterdam

WIDE-ENERGY-RANGE, HIGH-RESOLUTION MEASUREMENTS OF NEUTRON PULSE SHAPES OF POLYETHYLENE MODERATORS

Susumu IKEDA * and John M. CARPENTER

Argonne National Laboratory, Argonne, Illinois 60439, USA

Received 14 March 1985

We report measurements of the emission time distributions (pulse shapes) as functions of energy for neutrons emerging from two heavily irradiated, ambient-temperature polyethylene moderators in IPNS. A time-focused crystal spectrometer arrangement provided resolution such that instrumental broadening was insignificant; cooling the Ge monochromator to 10 K provided adequate reflectivity in the high energy region. Measurements covered the range $2.5 < E < 1000$ meV.

We introduce a novel set of functions which fit the pulse shapes over the entire range of energies with four wavelength-independent parameters.

1. Introduction

Knowledge of the shapes of pulses of neutrons emerging from pulsed-source moderators, as a function of energy, is essential for assessment of the resolution of pulsed-source time-of-flight instruments, and for the analysis of data. Polyethylene moderators are in common use since they are easy to fabricate and function adequately in present-day sources. Two ambient-temperature polyethylene moderators provide nine beams in the intense pulsed neutron source (IPNS) at Argonne National Laboratory [1]. These measurements provide precise information on the shapes of pulses from these moderators, over the entire range of energies for which they are used.

We accomplished this by using a time-focused crystal monochromator and detector arrangement which produced only negligible broadening of the pulses. The width of the pulse of primary, fast neutrons was very short, further guaranteeing negligible broadening of the observed pulses. To gain adequate intensity at high neutron energies, we used a Ge monochromator crystal, cooled to low temperature to improve the Debye–Waller factor.

In order to fit the measured pulse shapes we found it necessary to introduce a new but nevertheless simple form of function, which quite accurately fits the data over the measured range, $2.5 < E < 1000$ meV.

* Permanent address: National Laboratory for High Energy Physics, Oho-machi, Tsukuba-gun, Japan

2. Measurement of pulse shapes

We measured the neutron pulse shapes for two ambient-temperature polyethylene moderators. A time-focused crystal monochromator and detector [2,3] arranged at the monitor position of the low resolution medium-energy chopper spectrometer (LRMECS) and at the sample position of the single crystal diffractometer (SCD) of IPNS enabled these to extend up to nearly 1 eV. These spectrometers, respectively, view moderators designated "F" and "H".

2.1. The moderators

The moderators were originally of high density polyethylene $(CH_2)_n$, $\rho = 0.966$ g/cm^3. Due to nuclear heating, their temperature is approximately 50°C during operation. At the time of the measurements, the moderators had been in place for approximately one year and suffered substantial radiation damage due to a fast neutron fluence of approximately 5×10^{18} n/cm^2, corresponding to 8×10^{20} 450 MeV protons on the depleted U target. Shortly after completion of the measurements we removed and replaced the moderators. Tests indicated that the hydrogen-to-carbon ratio changed from H/C = 2.00 unirradiated to H/C = 1.56 ("F") and 1.50 ("H") after irradiation, while the mass density increased to 0.990 ("F") and 1.055 ("H"). The results are consistent with measurements carried out on polyethylene irradiated in the ZING-P′ prototype pulsed spallation source [4], and indicate substantial chemical alteration. Related changes are evident in the pulse shapes and spectra, as discussed below. How these

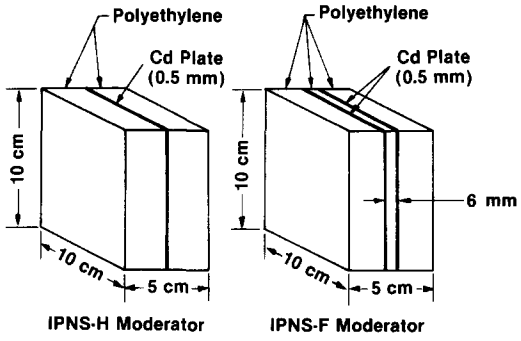

Fig. 1. The IPNS ambient-temperature polyethylene moderators. Both are decoupled from the surrounding graphite reflector by 0.5 mm Cd. F is viewed from both faces. H is reflected on the side opposite the viewed face.

effects set in as functions of time, dose and operating temperature, is not yet known.

Fig. 1 shows the shapes and sizes of the H and F moderators. The viewed layers of the F moderator (viewed from both sides), as defined by Cd heterogeneous poisoning, are slightly thinner than that of the H moderator (viewed from one side). Cadmium 0.55 mm thick decouples the moderators from the surrounding graphite reflector.

2.2. The neutron source

During these measurements, the IPNS operated at 30 Hz, delivering 450 MeV protons to the depleted uranium target. The width of the proton pulse (and approximately also of the primary, fast neutron pulse) was 100 ns (full width at 1/10 maximum). The time-average proton current was 12 μA.

2.3. The time-focused diffractometer

Fig. 2 schematically shows the experimental arrangement. This geometry must satisfy the following relations for time focusing (below, we have corrected a sign error in the earlier equations);

$$P \equiv L_f/L_i,$$

$$\tan\theta_M = \tfrac{1}{2}(1+P)\cot\theta_B,$$

$$\tan\theta_D = \tfrac{1}{2}(1+1/P)\cot\theta_B,$$

$$\cot\theta_C = \frac{\cos\theta_D \tan\theta_M + \sin(2\theta_B+\theta_D)}{2\sin\theta_B \sin(\theta_B+\theta_D)}. \quad (1)$$

To accomplish complete focusing, we have used planes not parallel to the cut face of the monochromator. In the case that a single crystal is cut parallel to planes with normal $S[h_1, k_1, l_1]$, while the reflection $R[h_2, k_2, l_2]$ is observed by the detector, the relation

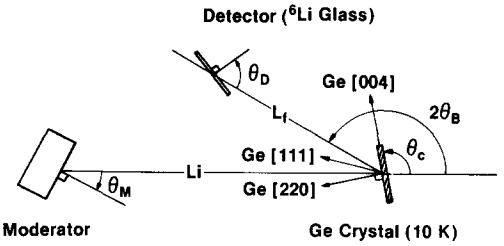

Fig. 2. Time-focused arrangement of moderator, monochromator and detector used in these measurements.

between the crystal orientation and the Bragg angle is

$$\theta_C = \theta_B + \cos^{-1}\left(\frac{\boldsymbol{S}\cdot\boldsymbol{R}}{|\boldsymbol{S}|\,|\boldsymbol{R}|}\right). \quad (2)$$

We used a 1 mm thick, 25 mm diameter single, deformed Ge crystal [5] cut perpendicular to $S[2, 2, 0]$. Germanium has the diamond cubic crystal structure and reflects neutrons under the conditions,

a) h_2, k_2, l_2 = all even and

$$h_2 + k_2 + l_2 = 4n \ (n = 1, 2, 3\cdots),$$

or

b) h_2, k_2, l_2 = all odd, (3)

Squared structure factors (therefore, approximately, reflectivities) for cases (a) are twice those for cases (b).

One constraint on our solution to eqs. (1) and (2) is that the beam holes view the IPNS moderators only at angles $\theta_M = 0°$, and $\pm 18°$ from the normal. Eqs. (1) imply that focusing is accomplishable for $\theta_M = 0$ only when $\theta_B = 90°$ (backscattering) and that focusing becomes progressively more awkward as the Bragg angle becomes smaller. At small Bragg angles, high reflectivity and low orders of reflection would correspond to energies below our range of interest. The presence of installed instruments required the use of of long initial paths L_i, contrary to needs for resolution and intensity. Final paths L_f needed to be short for reason of intensity; their lengths were ultimately determined by focusing conditions and the availability of appropriate reflecting planes in the monochromator. The motive to measure high neutron energies, however, would indicate use of small Bragg angles, since the same energies measured at large angles require high order reflections which are of low intensity due to the effect of the Debye–Waller factor. At the same time we do not wish to measure with too-high orders of reflection to avoid possible contamination of one reflection by another. Our solution was to reflect from (1, 1, 1) planes, at a fairly large Bragg angle $\theta_B = 60°$, and to improve the high-order reflectivity by cooling the crystal to 10 K. Table 1 gives details of our solution.

The crystal was installed at positions $L_i = 6.86$ m

Table 1
Parameters of the time-focused crystal spectrometer

$\boldsymbol{S}[h_1, k_1, l_1] = \boldsymbol{S}[2, 2, 0]$
$\boldsymbol{R}[h_2, k_2, l_2] = \boldsymbol{R}[1, 1, 1]$
$\cos^{-1}\left(\frac{\boldsymbol{S}\cdot\boldsymbol{R}}{|\boldsymbol{S}||\boldsymbol{R}|}\right) = 35.26°$
$\theta_M = 18°$, $\theta_B = 60°$
$\theta_D = 73°$, $\theta_C = 95.3°$
$L_i = 6.86$ m, $L_f = 0.686$ m ("H" moderator, SCD beam)
$L_i = 11.70$ m, $L_f = 1.17$ m ("F" moderator, LRMECS beam
$P = 0.1$ (both measurements)

from the H moderator (SCD) and $L_i = 11.70$ m from the F moderator (LRMECS), where the angles $\theta_M = 18°$. The detector was the scintillator and the shielding the same as used in Graham's experiments [3] to provide the needed rapid detector response and low background. (The time response of the detector is less than the neutron lifetime in the 6 w/o ^{6}Li-loaded scintillating glass, about 1/3 μs.) The 2 mm thick, 75 mm diameter detector was set at a scattering angle of 120° at the position where the distance ratio between incident flight path L_i and final flight path L_f, $P = L_f/L_i = 0.1$. The crystal angle θ_C and detector angle θ_D were 95.3° and 73°, respectively.

Since focusing applies only in the scattering plane, we estimated the geometric effects of time resolution due to out-of-plane defocusing and errors in our approximation to the focusing angles, by a Monte Carlo computer simulation. Fig. 3 shows the result for the $L_i = 6.86$ m case and for the Ge(1, 1, 1) reflection (corresponding to 2.53 meV). The resolution for higher energy and for the longer flight path can also be calculated since the resolution scales in proportion to the neutron wavelength and to the total length of the flight path. Table 2 summarizes the estimated full widths at half-maximum (fwhm) of the resolution for the allowed

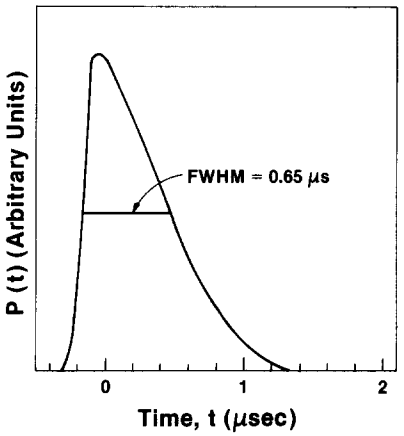

Fig. 3. Calculated time distribution representing the geometric contribution to the resolution in the time focusing arrangement. The results are for the Ge(111) reflection ($E = 2.53$ meV) and for $L_i = 6.86$ m, $L_f = 0.686$ m.

reflections Ge(1, 1, 1), Ge(3, 3, 3), etc. The fwhm's are insignificant. For example, the calculated values of resolution are about 0.65 μs for 2.53 meV and 0.03 μs for 1 eV, while the expected widths of the neutron pulses are about 50 μs for the energy region below 100 meV and about 2 μs for 1 eV, and observed rise times vary from about 20 μs for the lowest energy to about 1 μs for the highest.

Thus the time-channel width and detector response times are dominant in the resolution of our measurement. Choosing 0.25 μs channel width for $E \gtrsim 100$ meV and 1.0 μs for $E \lesssim 100$ meV, the effect of channel width is still small in relation to the measured neutron pulse widths and rise times. Therefore, we were able to analyze the measured neutron pulse shape without further consideration of the instrumental resolution.

We cooled the Ge crystal to about 10 K in order to gain higher intensity at the high energies of interest.

Table 2
Fwhm of calculated resolution and allowed reflections of Ge(n, n, n)

n	1	3	4	5	7	8	9	11
E_n (meV) [a]	2.53	22.3	40.5	63.3	124	162	205	306
Δt_{ch} (μs) [b]	1	1	1	1	0.25	0.25	0.25	0.25
Δt_{cal} (μs) [c]	0.65	0.22	0.16	0.13	0.09	0.08	0.07	0.06
n	12	13	15	16	17	19	20	21
E_n (meV)	364	428	569	648	731	913	1012	1116
Δt_{ch} (μs)	0.25	0.25	0.25	0.25	0.25	0.25	0.25	0.25
Δt_{cal} (μs)	0.05	0.05	0.04	0.04	0.04	0.03	0.03	0.03

[a] E_n: calculated in our geometry of $\theta = 120°$.
[b] Δt_{ch}: channel width used for our measurements.
[c] Δt_{cal}: fwhm of calculated resolution for $L_i = 6.86$ and $L_f = 0.686$ (for "H" moderator measurements; resolution is twice this figure for the measurements on the "F" moderator).

When $T = 300$ K, the exponent of the Debye–Waller factor $2W(T)$ is expressed by the high temperature expansion [6]

$$2W(T) = 6E_R kT/(k\theta_D)^2\left[1 + (\theta_D/T)^2 + \cdots\right],$$
$$2W(300) = 0.156E_R, \quad (4)$$

in which $E_R = \hbar^2 Q^2/2m$ is the recoil energy, $Q = 2\pi/d_n$ and $\theta_D = 374$ K = Debye temperature [7]. In the limit of $T \to 0$ K, the Debye–Waller factor is given as

$$2W(0) = 1.5E_R/(k\theta_D) = 0.0465E_R. \quad (5)$$

For example, assuming $E = 500$ meV, ($Q = 15.5A^{-1}$ in our geometry), the recoil energy is $E_R = 27.5$ meV, the Debye–Waller factor is approximately $\exp(-2W(300)) = 0.014$, while $\exp(-2W(0)) = 0.28$, and the intensity ratio $I(0)/I(300)$ is

$$I(0)/I(300) = \exp(-2W(0))/\exp(-2W(300)) \sim 20. \quad (6)$$

Thus, we obtained adequate intensity in the high energy region by cooling the Ge crystal to 10 K.

By these optimizations of the measurement geometry and by cooling the crystal, we obtained good data up to 16th order, corresponding to 650 meV in both measurements. In the LRMECS measurement, we even observed all the allowed reflections up to 20th order (~ 1 eV). Fig. 4 displays the full raw data from the F moderator. Figs. 5a and b respectively illustrate raw data from the H moderator, Ge(1, 1, 1) and Ge(16, 16, 16) reflections. The widths compare reasonably well with those of Graham [3], but are somewhat larger.

Small peaks are present corresponding to Ge(2, 2, 2) and Ge(6, 6, 6) in both measurements. These reflections are prohibited in the diamond structure, but are presumably caused by imperfections of the Ge crystal due to impurities or strains. Fig. 6 shows the fwhm of neutron pulses obtained from the raw measurements. At

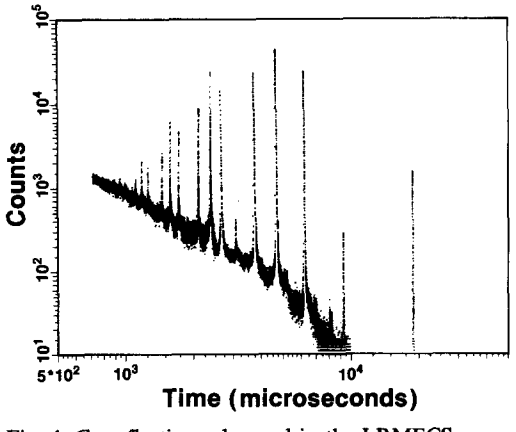

Fig. 4. Ge reflections observed in the LRMECS measurement with $L_i = 11.7$ m, $L_f = 1.17$ m.

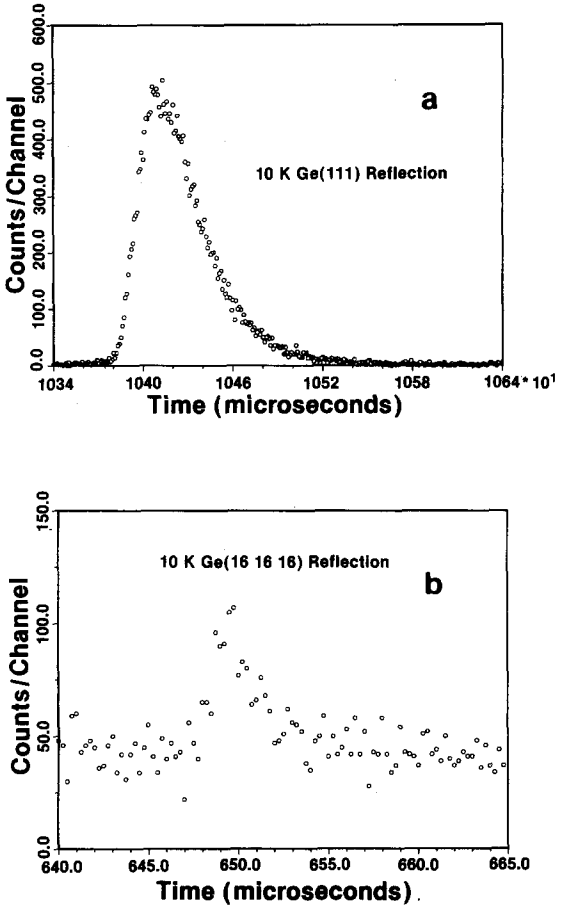

Fig. 5. Ge(n, n, n) reflection observed in SCD measurement: (a) Ge(1, 1, 1) and (b) Ge(16, 16, 16), $E = 2.53$ meV and 648 meV respectively.

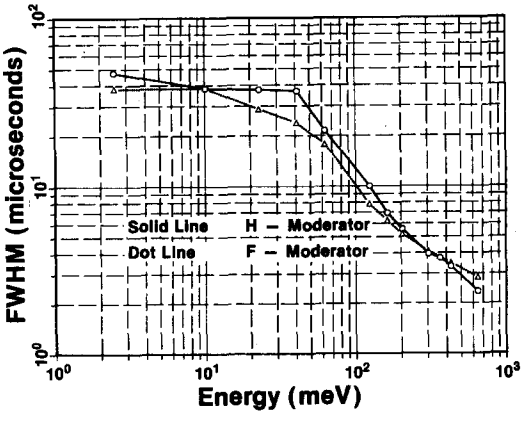

Fig. 6. Neutron pulse widths of IPNS H-moderator and F-moderator; (○) and (△) are observed values in both measurements.

this level of analysis, the results contain considerable statistical error. The widths of the neutron pulses from the F moderator are somewhat smaller than those from the H moderator in the energy region below 200 meV, even though both fwhm's have about the same values in the upper region. This is expected since the Cd poisoning is ineffective at the higher energies.

3. Analysis and discussion

A number of workers have used different functions for the analysis of neutron pulse shapes. For example, Jorgensen [8] used the function

$$\text{gauss}*[\theta(t)\exp(-k_1 t)+\theta(-t)\exp(k_2 t)] \quad (7)$$

to fit the pulse shape of powder diffraction data utilizing a room temperature polyethylene moderator. Here, "gauss" designates the function $\exp(-(t-t_0)^2)/2\sigma^2$ and the symbol "*" indicates convolution. $\theta(t)$ is the Heaviside function $\theta(x<0)=0$, $\theta(x>0)=1$. Carpenter et al. [9] used the sum of two decaying exponential functions to fit neutron pulse shapes from a liquid methane moderator,

$$\text{gauss}*\theta(t)[R\exp(-k_1 t)+(1-R)\exp(-k_2 t)]. \quad (8)$$

The Gaussian accounts partly for resolution effects, and partly describes the smooth initial rise of the pulse. We also tried to fit our data using these functions, but we were not successful.

The time distribution of neutrons coming from a hydrogenous moderator in the high energy region is expected to be of the form of a chi-squared distribution function (with six degrees of freedom)

$$\phi(v,t)=\frac{\Sigma v}{2}(\Sigma v t)^2\exp(-\Sigma v t) \quad (t>0), \quad (9)$$

where Σ is the macroscopic neutron scattering cross-section of the moderator ($\Sigma = 1.6\ \text{cm}^{-1}$ for polyethylene in the high energy limit) and v is the neutron speed. In this form, $\int_0^\infty \mathrm{d}t\,\phi(v,t)=1$. Strictly speaking, the equation describes the slowing-down time distribution of neutrons in an infinite medium of free protons at rest, with no absorption. However, Coceva et al. [10] have recently successfully fitted a function of this form to Monte Carlo simulations of the pulse from the ORELA target at high neutron energies.

This function describes a pulse shape which scales in a simple way according to neutron speed if Σ does not depend on v. Figs. 7 and 8 show the measured pulse shapes as a function of the time scaled by the neutron speed, the reduced time (actually a length). In both instances, peak values are normalized to 1. Fig. 7 shows

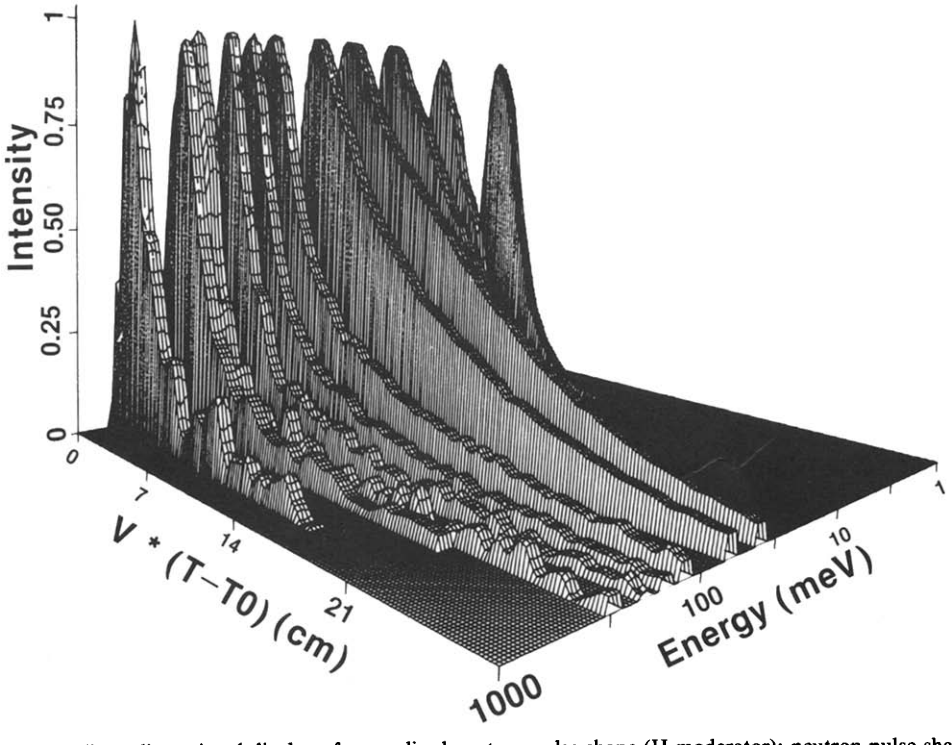

Fig. 7. Three dimensional display of normalized neutron pulse shape (H moderator); neutron pulse shapes are plotted on a reduced time scale $v(t-t_0)$, where v and t_0 are the neutron speed and the beginning time of the neutron pulse.

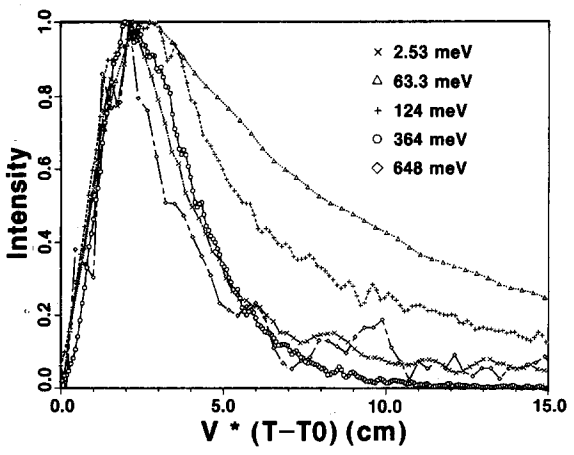

Fig. 8. Pulse shapes for several energies vs reduced time.

all the data for the H moderator in terms of the scaled time.

As seen in fig. 8, the pulse shape for 364 meV is almost the same as that for 648 meV, consistent with eq. (9) in this high energy region (scaling region), but the pulse shapes for neutrons in the region $E < 200$ meV are much different from those in the scaling region; the neutron pulse shape cannot be expressed as eq. (9) in this low energy region (nonscaling region).

We noticed that the rising part (before the peak point) as a function of reduced time in the nonscaling region is nearly invariant with energy even though the decaying part (after the peak point) is much different from that in the scaling region. Moreover, at long times the pulse shapes in the nonscaling region have the form ot the function $\exp(-\beta t)$, where β is independent of energy as expected [11]. These results suggested that the scaling component described by eq. (9) still exists even in the nonscaling region, but that the moderator has a characteristic storage time $(1/\beta)$, which dominates the decay in the nonscaling region.

Therefore, we introduce a new function,

$$\psi(v, t) = \int \mathrm{d}t' \phi(v, t')[(1-R)\,\delta(t-t') + R\beta\theta(t-t')\exp(-\beta(t-t'))]; \quad (t>0) \tag{10}$$

$$= \frac{\alpha}{2}\left\{(1-R)(\alpha t)^2 \mathrm{e}^{-\alpha t} + 2R\frac{\alpha^2\beta}{(\alpha-\beta)^3} \times \left[\mathrm{e}^{-\beta t} - \mathrm{e}^{-\alpha t}\left(1+(\alpha-\beta)t+\tfrac{1}{2}(\alpha-\beta)^2 t^2\right)\right]\right\}; \quad t>0, \tag{10'}$$

where $\phi(v, t)$ is the function given by eq. (9) with $\alpha = v\Sigma$ and R is the ratio of the area of the second term to the total area. $\delta(t-t')$ is the Dirac delta function. In this form, $\int_0^\infty \psi(v, t)\mathrm{d}t = 1$. The physical content of the function in eq. (10) is that slow neutrons are generateds by an initial source which is the slowing-down distribution expressed by eq. (9), while a part of them (in ratio R to the total) are stored in the moderator and decay with a time constant β. The first slowing-down term in eq. (10) represents neutrons which emerge in the process of slowing down before thermalization. The second term (storage term) represents neutrons which emerge after thermalization. As we show, the function in eq. (10) is quite consistent with the measured pulse shapes and moreover has the advantage over previously used ones, that it goes over at both the high-energy and the low-energy, long-time limits to forms consistent with theoretical expectations. The functions ϕ and ψ have very simple Laplace transforms, a property that may be useful when these are convoluted with other causal functions. This might be required, for example, in calculating time-of-flight powder diffraction profiles.

Pulse shapes of both measurements were fitted maintaining all parameters of eq. (10), Σ, β, R and a time delay t_0 as free parameters for each energy. The time delay, which represents the flight time from moderator to detector plus a fixed shift of the time origin, was a strictly linear function of the wavelength, and correlated exactly with known flight path lengths and time-triggering offsets. The quality of fits to the measured shapes was excellent, except for the reflection Ge(4, 4, 4) in the SCD measurement. The pulse shape for this reflection has a small hump on the decreasing side. We tried to reproduce the hump as due to multiple scattering of neutrons in the Ge sample and the Al sample cell, but we could not explain a hump of such magnitude on that basis. This effect might come from a property of the SCD neutron flight path such as air scattering, or from neutrons scattering from the iron collimator elements in the beam hole. To varying extents in the two measurements and at different energies, a small component of intensity appears before the pulse and (at high energies) after the pulse. We suspect that this is due to inelastic, forward scattering of neutrons in the air-filled portions of the flight path.

Fig. 9 shows an example of the results of fitting the Ge(5, 5, 5) peak in the LRMECS beam. This figure indicates well that the slowing-down term is important in determining the rising part and that the storage-term shape is dominant in the decaying part at this wavelength. Fig. 10 shows the neutron wavelength dependence of β and Σ. The parameter Σ can be fitted as a function of wavelength λ by a form

$$\Sigma = \left(S_1^2 + S_2^2\lambda^2\right)^{1/2}. \tag{11}$$

Fig. 10 also shows the fitted functions. The values of S_1 and S_2 are

$S_1 = 0.98\ \mathrm{cm}^{-1}$,

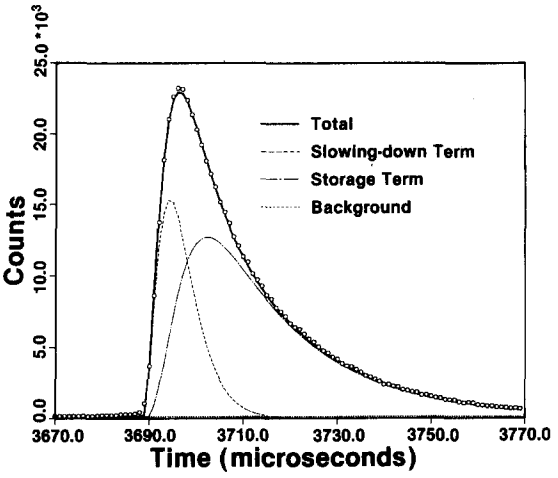

Fig. 9. Ge(5, 5, 5) reflection for F moderator. The solid line is calculated by eq. (10) with parameters $\Sigma = 1.05$ cm^{-1}, $\beta = 0.0487/\mu$s and $R = 0.72$.

$S_2 = 0.27$ cm^{-1}A^{-1} (for H moderator);

and

$S_1 = 1.0$ cm^{-1},

$S_2 = 0.38$ cm^{-1}A^{-1} (for F moderator). (12)

β is almost constant in the range of $0.4 < \lambda < 6$ Å as

$1/\beta = 24.1$ μs (for H moderator),

and

$1/\beta = 21.5$ μs (for F moderator). (13)

At small wavelengths, the fitted β parameter is larger than the value fitted at long wavelengths which is evidence of the diminished effectiveness of cadmium decoupling at short wavelengths. This is also evident in the amplitude ratio factor R, for which the data at short wavelength lie a little above our smooth fitted function. Thus, we conclude that the effect of the graphite reflector not being decoupled at short wavelengths is to introduce a "tail" on the pulse shape. The tail decays faster than the "storage" term which is dominant at low energies but seems to be taken up in the fitting procedure as a component of that form. The overall fitted functions β and R do not reflect this effect, and we interpret our overall fitted results as applying to ideally decoupled moderators.

For protons at the density of unirradiated polyethylene, we expect that $\Sigma = 1.6$ cm^{-1} in the high energy limit, but the value of Σ obtained by fitting is only ~ 0.6 times the expected value of 1.6 cm^{-1}. It seems that the hydrogen concentration in the polyethylene moderator has been decreased by neutron and γ ray irradiation from the target.

Fig. 11 shows the neutron wavelength dependence of the ratio factors R, given by fitting the pulse shapes for both moderators. We have represented these values simply in terms of a Boltzmann function as

$$R = \exp(-E/E_0), \quad (14)$$

where E is the neutron energy and E_0 a fitting parameter. The value of E_0 is almost the same for both moderators; the solid line in fig. 11 is the curve calculated by eq. (14) with $E_0 = 190$ meV.

Figs. 12a and b show the overall pulse shape function calculated from the fitted functions. The results are normalized to unity at the peak.

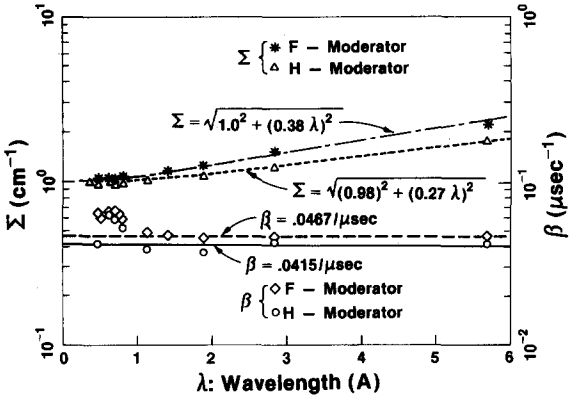

Fig. 10. Wavelength dependence of Σ and β: chain-dash line and dotted lines are the fitting lines for Σ of F and H moderators respectively. Dashed and solid lines indicate $\beta = 0.0467/\mu$s and $\beta = 0.0415/\mu$s respectively. Note the rise above the constant value which occurs at short wavelengths.

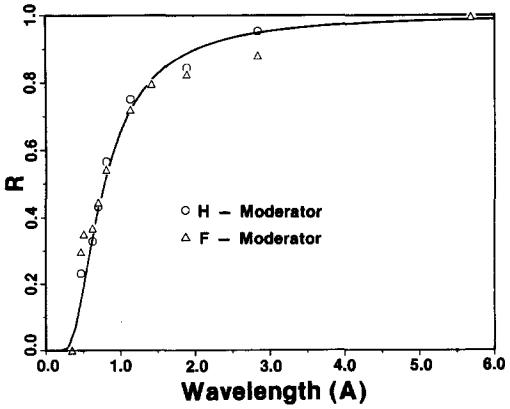

Fig. 11. Wavelength dependence of R. The solid line is a Boltzmann function $\exp(-E/E_0)$ with $E_0 = 190$ meV. Note the rise above the smooth fitted function which occurs at short wavelengths.

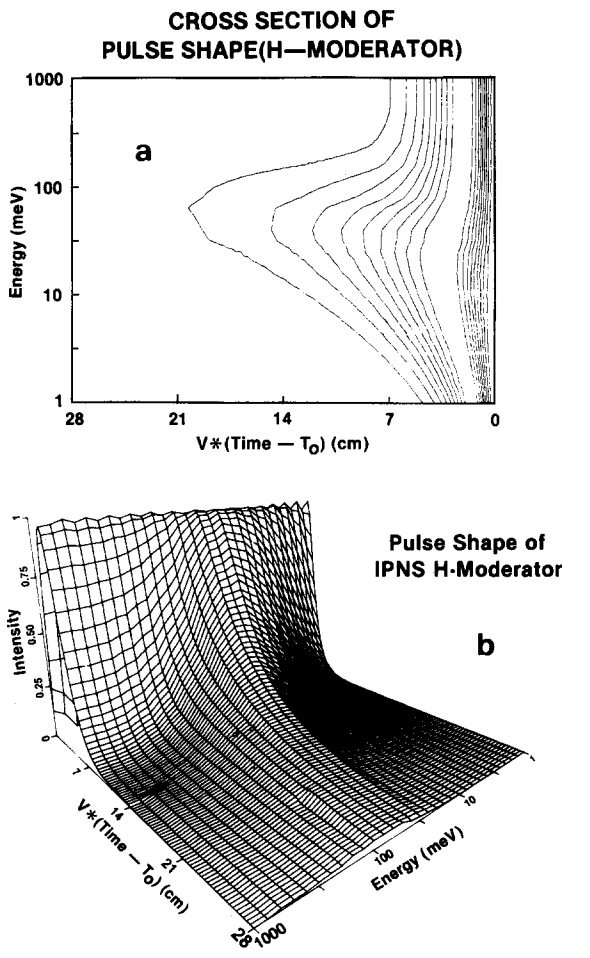

Fig. 12. The pulse shape function of the H moderator. (a) Contour plot (the peak contour is absent) and (b) three dimensional plot. The plotted result is that calculated from the fitted functions (see text).

4. Measurement and fitting of the spectra

Time-of-flight analysis of direct beams provided the energy distribution of the neutrons from the moderators. When measured by a detector of area A, at distance L from the source, whose efficiency is $\eta(E)$, the total count per unit time-of-flight t, in measuring time T is

$$c(t) = A\eta(E)\frac{\bar{i}(E)}{L^2}\left|\frac{dE}{dt}\right|T, \tag{15}$$

where

$$E = \frac{m}{2}\left[\frac{L}{t-\bar{t}(E)}\right]^2, \tag{16}$$

and $\bar{i}(E)$ is the time-average number of neutrons emerging from the viewed moderator surface, per unit solid angle, per unit time, per unit energy (the "beam current"). Here, $\bar{t}(E)$ is the mean time following the time origin, at which neutrons of energy E emerge from the moderator surface, and dE/dt is the Jacobian. Strictly, one should infer E from eq. (16), and compute the Jacobian

$$\frac{dE}{dt} = \left[\frac{t-\bar{t}(E)}{2E} - \frac{d\bar{t}(E)}{dE}\right]^{-1}, \tag{17}$$

but since $\bar{t}(E)$ is slowly varying and since $L \gg v\bar{t}(E) \lesssim 5$ cm in our measurements, we ignore $\bar{t}$ in our calculations. We used uncalibrated, low-efficiency, "pancake" $^{10}BF_3$ detectors, for which $\eta(E) \propto \lambda$, and have fitted the form

$$\bar{i}(E) = \bar{i}_{Th}\frac{E}{E_T^2}e^{-E/E_T} + \bar{i}_{epi}\frac{\Delta(E)}{\Delta(E_0)}\frac{1}{E}\left(\frac{E}{E_0}\right)^{\alpha} \tag{18}$$

to the measured beam current. Here, $\bar{i}_{Th}$ is the time-average integrated Maxwellian beam current, E_T is the mean energy of the Maxwellian component ($E_T = k_B T_{eff}$, where T_{eff} is the effective spectral temperature), and $\bar{i}_{epi}$ is the time-average epithermal beam current (the current per unit lethargy ln E/E_0, at reference energy E_0). $\Delta(E)$ is the "joining function" for which we adopt Taylor's [9] form

$$\Delta(E) = (1 + e^{a\lambda - b})^{-1}, \tag{19}$$

and α is the leakage exponent. We fitted Wescott's [12] joining function $\Delta(E) = [1 + (E_{co}/E)^7]^{-1}$ with similar, but slightly poorer results. Table 3 gives the fitted parameters for F and H moderators. The parameters describing the spectrum in the epithermal region are subject to error because the monitor counters do not function properly at short times following the initial source pulse.

As expected because the moderators are quite similar, the spectra of the two moderators are nearly identical. The mean spectral energies are in reasonable agreement with the data of Graham [3] for moderators of this size, although the physical temperatures of the present moderators are somewhat higher, and the thermal-to-epithermal flux ratios somewhat smaller, presumably because they have suffered substantial radiation damage. The table also gives the "cutoff energy" of the epithermal spectrum

$$\Delta(E_{co}) \equiv 1/2, \tag{20}$$

$$E_{co} = \left(\frac{h^2}{2m}\right)\lambda_{co}^{-2}, \tag{21}$$

$$\lambda_{co} = b/a, \tag{22}$$

and the ratio E_{co}/E_T. The epithermal cutoff energy defined in this way E_{co} is similar to that determined using Wescott's joining function, i.e. $E_{co}/E_T \approx 5$, and, moreover, equal to the value of parameters E_0 obtained in the previous section.

Table 3
Fitted parameters for the F and H moderators

Moderator	E_T [meV]	T_{eff} [K]	i_{Th}/i_{epi}	a [Å^{-1}]	b	E_{co} [meV]	E_{co}/E_T	α
F	40	464	2.29	8.74	5.74	190	4.75	0.01
H	37	429	3.36	8.74	5.74	190	5.14	0.01

There is remarkably no obvious evidence of the falloff of the cadmium (used for poisoning and decoupling) cross section, except the rise of the β parameter and the ratio R at short wavelengths.

5. Conclusion

We have demonstrated a method for measuring the shapes of moderator neutron pulses for energies up to 1 eV, with high resolution. The data for two polyethylene moderators require and provide the basis for fitting by functions of a new form. Results indicate substantial radiation degradation of the polyethylene.

We acknowledge with gratitude the assistance of the IPNS operations staff in setting up our apparatus. One of us (S.I.) gratefully acknowledges the hospitality of the Argonne National Laboratory during his term as visiting scientist there. Work supported in part by the US Department of Energy.

References

[1] J.M. Carpenter, G.H. Lander and C.G. Windsor. Rev. Sci. Instr. 5 (1984) 1019.
[2] A. Holas, Dubna Report INR No. 742/II/PS (1966); Nukleonika 13 (1968) 871; J.M. Carpenter, Nucl. Instr. and Meth. 47 (1967) 179.
[3] K.F Graham and J.M. Carpenter, Nucl. Sci. Eng. 49 (1972) 418; Nucl. Instr. and Meth. 85 (1970) 165.
[4] J.M. Carpenter and the IPNS Program Staff, Proc. 4th Meeting Int. Collaboration on Advanced Neutron Sources, Tsukuba, Japan (1980) Report of the Japanese Laboratory for High Energy Physics (KEK), KENS Report III (1981) p. 105.
[5] C.S. Barrett, M.H. Mueller and L. Heaton, Rev. Sci. Instr. 34 (1963) 847.
[6] W. Marshall and S.W. Løvesey, Theory of Thermal Neutron Scattering (Oxford University Press, Oxford, 1971).
[7] American Institute of Physics Handbook, ed., D.E. Gray.
[8] J.M. Carpenter, M.H. Mueller, R.A. Beyerlein, T.G. Worlton, J.D. Jorgensen, T.O. Brun, K. Sköld, C.A. Pelizzari, S.W. Peterson, N. Watanabe, M. Kimura and J.E. Gunning, Proc. Neutron Diffraction Conf., Petten, The Netherlands, and F. Kropff, J.R. Granada and R.E. Mayer, Nucl. Instr. and Meth. 198 (1982) 515.
[9] J.M. Carpenter, R.A. Robinson, A.D. Taylor and D.J. Picton, Nucl. Instr. and Meth. A234 (1985) 542.
[10] C. Coceva, R. Simonini and D.K. Olsen, Nucl. Instr. and Meth. 211 (1983) 459.
[11] See, for example, M.M.R. Williams, The Slowing Down and Thermalization of Neutrons (North-Holland, Amsterdam, 1966).
[12] C.H. Wescott, Chalk River Report Number CRRP-960 and AECL-1101, 3rd ed. (1969).